Journal of Gerontology: BIOLOGICAL SCIENCES
1998, Vol. 53A, No. 5, B369–B379

Decreased Axosomatic Input to Motoneurons and Astrogliosis in the Spinal Cord of Aged Rats

Susanna Kullberg, Vania Ramírez-León, Hans Johnson, and Brun Ulfhake

Department of Neuroscience, Karolinska Institutet, Stockholm, Sweden.

An increasing body of evidence indicates that aging-related impairments of nervous functions are caused by damage to neuron integrity rather than by loss of neurons. By using electron microscopy, we have examined axosomatic boutons on spinal cord motoneurons derived from aged and young adult Sprague-Dawley rats. The main finding was that about half of the examined motoneuron somata from aged rats had a reduced (50%) bouton coverage, which seemed to be caused by a smaller number of axosomatic bouton profiles. Long streches of the cell body plasma membrane were apposed by pale processes, and immunolabeling for glial fibrillary acidic protein (GFAP) disclosed that a number of the aged motoneurons appeared embedded in GFAP immunopositive processes. Lumbar motoneurons seemed to be more severely affected than cervical motoneurons. At the ultrastructural level, affected motoneurons disclosed plasma membrane irregularities with appendages/sprout-like extensions that in some cases were sites for axosomatic contacts.

WITH advancing age, the incidence of neurodegeneration and clinical signs of nervous disorders such as sensory-motor impairment(s) increase. Aging of the nervous system has been associated with decreased numbers of neurons, axon lesions, and astrogliosis. A general loss of neurons during aging has more recently been challenged (1–10), and a reduction in the number of neurons associated with aging has only been established for discrete regions of the brain and, thus, seems to be highly selective (11–15). In contrast, changes in aging neurons such as reduction/loss/remodeling of dendrites/spines and reduction/degeneration/dystrophy of axons have been firmly established (refs. 5 and 16–21; for reviews, see refs. 22 and 23). Damage of axons also includes the terminals, and dystrophy, degeneration, and loss of axon terminals have been reported in a number of studies [refs. 24–33; see also a review by Cotman and Holets (23)]. Studies examining loss of synaptic input with age have mainly been executed on tissue from hippocampus, various cortical regions, and the cerebellum (for references, see above). There seem to be no data available on the spinal cord motor nucleus, despite the frequent occurrence of motor incapacities that come with age (34–38). Furthermore, immunohistochemical studies have shown extensive axon degeneration/dystrophy in specific inputs to the motor nucleus [20,39–41; see also Bergman et al. (42)]. Therefore, we have used electron microscopy to examine boutons apposing cervical and lumbar motoneuron somata in 30-month-old (median survival age cohort) and young adult (3-month-old) Sprague-Dawley rats. In addition, immunohistochemistry for glial fibrillary acidic protein (GFAP) (43) and Marchi staining of myelin were used to verify astrogliosis and changes in myelin staining.

Material and Methods

Experimental Animals

In this study, male Sprague-Dawley rats (SD; strain: Bkl:SD), including a total of eight young adult (2–3 months old; body weight: 200–300 g) and eight aged rats (30 months old; body weight: 450–650 g), were used. The animals were delivered by a local breeder (B&K, Stockholm, Sweden) at 2 months of age and thereafter kept under standardized barrier-breeding conditions at our department (12 h light/12 h dark cycle) with free access to water and food (R70, with reduced protein content; Lactamin, Vadstena, Sweden). Under these conditions the median life span is about 30 months (±2 months across cohorts) for both males and females (44–47). Based on this, the 30-month-old rats were defined as "aged."

Rats show a progressive deterioration of motor behavior during aging (34–37,39,48), with symptoms usually starting during the third year of life and mainly affecting the hind limbs ("posterior paralysis"). All aged rats used in this study disclosed signs of behavioral disturbances, defined according to a previously described staging protocol (38). Briefly, the symptoms were most evident in the hind limbs and ranged from a moderate muscular atrophy and an adduction insufficiency in the least affected cases (stage I), to a more or less complete paralysis of the hind limbs with severe wasting of the hind-limb muscles in the most severely affected animals (stage III). The aged rats used in this study were in stages II or III.

Tissue Preparation for Electron Microscopy and Marchi Staining for Light Microscopy

Four aged and four young adult rats were deeply anaesthetized with pentobarbital (40 mg/kg). Following a brief rinse with Tyrode's solution for 15 sec, the tissue was fixed by intravascular perfusion through the descending aorta with 4% glutaraldehyde and 0.5% paraformaldehyde in 0.1 M phosphate-buffered saline (PBS), pH 7.4 (5–10 min). The spinal cord was quickly removed and placed in a fresh fixative for 4 h. The isolated C_{5-8}, midthoracic, and $L_{2,4-6}$ segments were stored in 300 mOsm PBS (pH 7.4) at 4°C

overnight and then cut on a Vibratome (Oxford Lab, San Mateo, CA) in 50-μm-thick transverse sections. Sections from two aged and two young adult animals were treated with 1% OsO_4 in PBS for 1 h, dehydrated in a graded series of alcohol (with a final step in 100% acetone, 20 min), and embedded in Durcupan ACM (Fluka, Buchs, Switzerland). The embedded sections were inspected in the light microscope, and appropriate areas of the ventral horn motor nuclei were trimmed out and subjected to ultrathin sectioning with an LKB Ultratome (LKB, Gaithersburg, MD) and mounted on formvar-coated nickel slot grids.

From the remaining animals, Vibratome sections from C_{5-8}, midthoracic, and $L_{2,4-6}$ spinal cord levels were incubated in Marchi's solution [one part 1% osmium and three parts 1% $KClO_3$ dissolved in 300 mOsm/liter phosphate buffer (49,50)] for 18 h, dehydrated in alcohol (with a final step in 100% acetone, 20 min), and embedded in Epon (Agar 100 resin; Agar Aids, Essex, U.K.) between plastic foils for light microscopy. These sections were used to study Marchi positive bodies (MPBs) in the white matter.

Electron Microscopic Analysis

Axonal boutons in direct contact with a total of 8–12 large cells in the cervical and lumbar lateral motor nucleus, respectively, were analyzed qualitatively and quantitatively in two aged and two young adult rats. In all, 40 neurons were examined in the electron microscope, and photographs were taken at ×3000 magnification for the quantitative analysis (final magnification, ×12,000). The neurons were considered to be α-motoneurons because they were located in the lateral motor nucleus and had a mean cell body diameter exceeding 30 μm in the nuclear plane. All quantitative measurements were performed with a digitizing tablet (Summagraphics, SummaSketch Plus, Fairfield, CT) and commercially available software (Bioquant, R&M Biometrics, Nashville, TN; Excel, Microsoft Corp., Redmond, WA; ProStat, Poly Software Intl., Salt Lake City, UT; Kaleidagraph, Synergy Software, Reading, PA). For each of the 40 cells, the following parameters were recorded: (i) the total length of the postsynaptic membrane, (ii) the total number of synaptic boutons in direct apposition to the cell body membrane, and (iii) the total proportion of the cell membrane covered by synaptic boutons (percent synaptic covering) (51). In addition, the cell body diameters of these neurons were measured in the nuclear plane by using adjacent semi-thin sections (0.5–1 μm) counterstained with toluidin blue.

Immunofluorescence Histochemistry

Four aged and four young adult rats deeply anaesthetized with chloral hydrate (300 mg per kg^{-1} i.p.) were perfused transcardially with warm (37°C), Ca^{2+}-free Tyrode's solution followed by cold fixative (4°C) containing 4% (w/v) paraformaldehyde and 0.2% (w/v) picric acid in 0.1 M PBS (pH 7.2) (52,53) for 8 min. Cervical (C_{5-7}) and lumbar (L_{4-5}) spinal cord segments were dissected out, immersed in fresh fixative for 90 min, and stored in 10% sucrose buffer solution containing 0.01% sodium azide (Sigma, St. Louis, MO) and 0.02% Bacitracin (Bayer, Leverkusen, Germany) overnight at 4°C. Sections were cut at 14 μm in a cryostat (Dittes, Heidelberg, Germany) and thaw-mounted onto chrome-alum gelatin coated slides. Indirect immunohistochemistry for visualization of GFAP-immunoreactivity (IR) was performed according to the technique of Coons and collaborators (54). After rehydration in 0.1 M PBS the sections were preincubated for 1 h at room temperature in PBS containing 10% normal donkey serum and 0.3% Triton X-100 and then incubated for 72 h at 4°C in a humid chamber with a mouse monoclonal antibody to GFAP (dilution 1:50; Boehringer Mannheim, Stockholm, Sweden) in PBS containing 1% bovine serum albumin, 0.3% Triton X-100, 0.01% sodium azide, and 0.02% Bacitracin (55). After incubation with the primary antiserum the sections were rinsed several times in PBS, transferred to a humid chamber, and incubated at 37°C for 30 min with a fluorescein isothiocyanate (FITC)-conjugated donkey anti-mouse high affinity purified antiserum (1:40; Jackson ImmunoResearch Laboratories, Inc., West Grove, PA). The sections were rinsed in PBS and mounted in glycerol/PBS (3:1) containing 0.1% *p*-phenylenediamine to retard fading (56,57). The specificity of the GFAP antibody has been characterized previously (58). Furthermore, the general labeling pattern agreed with previous studies using this antibody, and omission of the primary antibody resulted in no labeling.

CLSM and Light Microscopy

The tissue sections were examined in either a Nikon Microphot-FX epifluorescence microscope equipped with the proper filters for FITC-fluorescence (filter cube B-2A; 510-nm dichroic mirror; 450- to 490-nm excitation filter; 520- to 560-nm barrier filter; and 550-nm extra barrier shortpass filter), or a Sarastro 1000 confocal laser scanning microscope (CLSM). Briefly, the 488-nm line of an argon ion laser was used as excitation light, and the FITC-fluorescence was collected through a dichroic mirror (split wave length, 500 nm) and a long pass filter (LP, 515 nm). The images were recorded with a ×40/1.0 oil-immersion planapochromate objective with a depth resolution of ≈ 2 μm (59). The lateral pixel spacing was set to 0.25 μm and the *z*-axis stepping size to 0.4 μm. A series of 20 consecutive optical sections were recorded from each specimen for each image stack, thus covering a tissue depth of 8 μm. Photomicrographs were taken in the light microscope with black-and-white Kodak Technical Pan (processed as 400 ASA, Kodak, Rochester, NY), and digital images were printed on a Kodak printer.

Quantitative Analysis of MPBs

Five sections from cervical, thoracic, and lumbar level of the spinal cord, derived from two animals in each age group (see above), were used for light microscopical counting of MPBs. MPBs are defined as rounded or sometimes ellipsoidal black bodies with a diameter ≤20 μm. MPBs have been suggested to represent degenerated myelin, taken up by microglial cells in parallel with a structural or chemical transformation (60). MPBs were counted in six regions of the white matter at each spinal cord level (see Figure 5D) using an eye-piece grid and a ×60/1.4 Nikon oil-immersion planapochromate objective. All MPBs throughout the depth of the section within the grid were counted. In the counting, no distinction was made between MPBs and Marchi-posi-

tive granules (60). Each region measured 180 × 180 μm and had a thickness of 50 μm.

Statistical Analysis

Analysis of variance (ANOVA) with multiple comparison (Fisher's LSD test) was used to test differences between data from the two age groups. Test of difference between two samples was accomplished by the nonparametric Mann-Whitney U test. Data clustering was performed using K-mean cluster analysis. The χ^2 was used to test bin data. H_o was rejected at $p > .05$, and the levels of significance were indicated in tables and illustrations as follows: $p > .05$ = NS, $p < .05$ = *, $p < .01$ = **, $p < .005$ = ***. Correlation analysis was performed using linear least-square regression (significance was set to $r^2 \geq .50$).

Results

General Observations

Examination of semi-thin sections in the light microscope (Figure 1A) revealed aggregates of lipofuscin-like granules in all aged motoneurons. Except for the age pigments, however, no conspicuous difference in the gross morphology of aged compared to young adult motoneurons could be detected. Measurement of the mean cell body diameter of the motoneurons subjected to synaptological analysis revealed no statistically significant difference between the two age groups (Table 1). At the electron microscopic level, however, it became evident that many aged motoneurons differed in appearance based on the surface membrane contour and the membrane coverage. One group of aged motoneurons closely resembled young adult motoneurons, showing a fairly smooth cell body outline apposed by numerous boutons (Figure 1 A–C). The second group disclosed profound irregularities along the plasma membrane (Figure 1 A, B, and D), with numerous small extensions (appendages) resembling sprouts. Such processes were occasionally involved in synapse formation with apposing boutons. Long stretches of the cell body membrane appeared vacated of apposing boutons and were instead covered by pale processes. Motoneurons with this abberant or "reactive" appearance were intermingled with motoneurons that had a normal appearance (Figure 1 A and B). Normal and reactive motoneurons were seen in both the cervical and lumbar spinal cord in the two aged rats. Reactive motoneurons were not encountered in specimens from the young adult rats.

Axosomatic Boutons on Motoneurons

Some of the quantitative data have been compiled in Table 2. Considering the whole sample from both age groups, the ANOVA revealed a significant decrease in both the number of boutons per 100 μm soma membrane length ($p < .05$) and the percentage membrane covering by boutons ($p < .001$) in aged rats, whereas the difference in mean length of bouton apposition was not significant ($p > .05$). As evident from the data in Table 2, aged rat Ag1 showed a more marked decrease of the two parameters than aged rat Ag2 when compared to the young adult controls (Fisher's LSD). However, there was no significant difference within the age groups.

In the subsequent analysis, aged and young adult rat motoneurons, respectively, were partitioned in cervical and lumbar motoneurons. Because no statistically significant difference was evident between animals within each age group, data were pooled. The data have been plotted in the diagrams of Figure 2 A and B. They show that the results from the unpartitioned data sets (Table 2) also were valid for cervical and lumbar motoneurons, separately. However, the aging-related decrease in bouton apposition parameters was less pronounced in cervical motoneurons compared to lumbar motoneurons, indicating that lumbar motoneurons are more severely affected at this age. This difference could not be explained by bias caused by the small difference between rats Ag1 and Ag2, because Ag1 contributed with four neurons to both the cervical and the lumbar motoneuron sets. The diagrams also reveal that aged motoneurons are not a homogeneous group deviating from young adult motoneurons. It is clear (Figure 2 A and B) that a subset of both cervical (50%) and lumbar (40%) motoneurons in the aged rats have values for the measured bouton apposition parameters that are similar to those seen in young adult rats. Cluster analysis of the entire sample of motoneurons (Figure 2B), revealed one cluster around 53% membrane covering by boutons and another cluster centered around 31% membrane coverage. One young adult cervical motoneuron, six aged cervical motoneurons, and six aged lumbar motoneurons belonged to the cluster with the lower covering values.

Among the aged motoneurons (Figure 2C) there was no significant covariation between bouton apposition length, on one hand, and the number of boutons per unit membrane length, on the other (fraction of explained variance: 7–17%, $p > .05$). In fact, a number of the motoneurons with the smallest values for bouton numbers (Figure 2C) or bouton coverage (data not shown) disclosed values for bouton apposition length coinciding with the average value recorded in young adults.

GFAP-like IR

To further analyze the increased covering of motoneurons by pale processes, we used immunohistochemistry for GFAP. The labeling pattern for GFAP-like immunoreactivity (LI) showed a robust increase throughout the gray matter of aged rats as compared to young adult rats (Figure 3). Around a number of the large neurons in the lateral motor nucleus of the aged rat, presumably motoneurons, a very dense accumulation of GFAP-IR processes could be seen (Figure 3 A and B and Figure 4 A and B).

The labeling for GFAP also showed a conspicuous increase in certain regions of the white matter, such as the dorsal column (Figure 3 D and H) and outer part of the lateral funiculus (Figure 3 A and E).

MPBs

The Marchi-stained spinal cord sections from the aged rats (Figure 5 A and B) showed the occurrence of numerous MPBs and cystic enlargements in the white matter. MPBs were of variable size, ranging in diameter from about 10 μm, down to the resolution of the microscope, i.e., ≈0.3 μm. The occurrence of MPBs varied strongly from region to

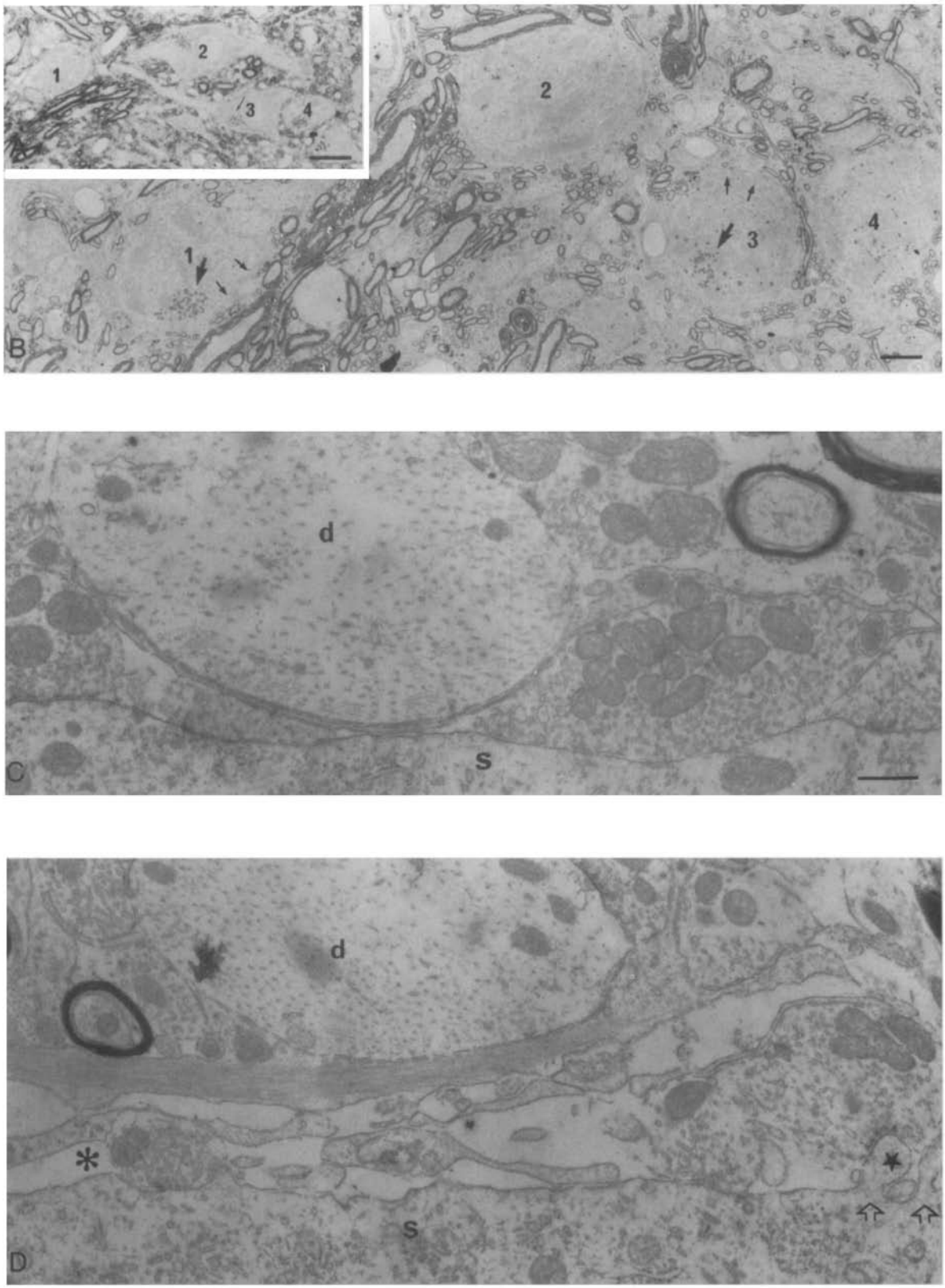

Figure 1. Light and electron micrographs from the lateral portion of the lumbar motor nucleus of an aged rat. (**A**) An overview (×10) taken from a semi-thin toluidin blue-stained section with four clearly visible neuronal cell bodies. Note the presence of lipofuscin-like granules in all neuronal profiles (thin arrow). (**B**) The same region as in **A**, from an adjacent ultrathin section taken at ×600 where all four neurons could be seen. Large arrows indicate lipofuscin-like granules. (**C** and **D**) High power electron micrographs from neuron 1 and 3, respectively, showing the plasma membrane regions spanning the distance between the small arrows in **B**. Note the difference in plasma membrane appearance and bouton coverage between neuron 1 (**C**) and neuron 3 (**D**). Neuron 1 is indistinguishable from young adult motoneurons, whereas neuron 3 shows an irregular plasma membrane contour with numerous extensions (star), few apposing boutons and extensive coverage by pale processes (asterisk). The dendrite and myelinated axon located nearby in **D** have a normal appearance. [Bars = 40 μm (**A**), 10 μm (**B**), and 0.5 μm (**C** and **D**).]

Table 1. Cell Body Diameter of Young Adult and Aged Motoneurons (μm)

	Cervical		Lumbar	
	Ad	Ag	Ad	Ag
Mean	52.6	47.5	47.8	47.8
SEM	2.6	2.7	2.7	3.4
Median	54.8	48.4	52.5	48.4
Range	39–63	36–61	34–55	30–60
n	10	10	10	10

Note: Ad, young adult; Ag, aged.

Table 2. Quantitative Data of Axosomatic Boutons on Motoneurons

Animal	No. Cells	Apposition (μm)	No. Bouton/ 100 μm	% Membrane Covering
Ad 1	8	1.16 ± 0.19	44.9 ± 5.3	51.8 ± 8.5
		1.21	46.0	53.2
Ad 2	12	1.21 ± 0.21	45.0 ± 4.7	53.6 ± 5.5
		1.21	45.6	49.2
Ad 1 + 2	20	1.19 ± 0.20	44.9 ± 6.2	52.9 ± 7.6
		1.20	46.1	53.2
Ag 1	8	1.06 ± 0.22	33.8 ± 10.6	35.5 ± 11.5
		1.13	31.7	33.7
Ag 2	12	1.05 ± 0.13	39.0 ± 10.5	40.1 ± 9.8
		0.95	44.5	41.0
Ag 1 + 2	20	1.05 ± 0.19$^{n.s.}$	36.9 ± 10.2*	38.3 ± 10.7***
		1.08	39.2	38.9

Ad = young adult, Ag = aged. Mean, standard deviation, and median values have been indicated.

region of the white matter (see Figure 5 D and E) but was generally several times higher than that found in normal young adult rats. The white matter regions with the largest number of MPBs in the aged rats were the medial portion of the dorsal column and the outer part of the dorsolateral funiculus (Figure 5 A–C). However, in the lumbar spinal cord of aged rats, the most medial portion of the dorsal columns had a pale appearance and thus seemed almost devoid of myelin (Figure 5B).

Discussion

The main finding of this study is that about half of cervical and lumbar motoneurons in aged rats seem to have lost about 50% of their axosomatic boutons. Long stretches of the cell body plasma membrane, seemingly vacated of boutons, were apposed by pale processes. Labeling for GFAP-like IR showed that a number of motoneurons appeared as "embedded" in GFAP immunopositive processes. At the ultrastructural level, the plasma membrane of such neurons showed frequent irregularities, such as sprout-like extensions that, in some cases, were sites of axosomatic contacts. Aged motoneurons with this kind of reactive appearance were intermingled with motoneurons that had a normal pattern of apposing boutons and a fairly smooth plasma membrane contour, indicating that these aging-related changes are selective within the population of spinal cord motoneurons.

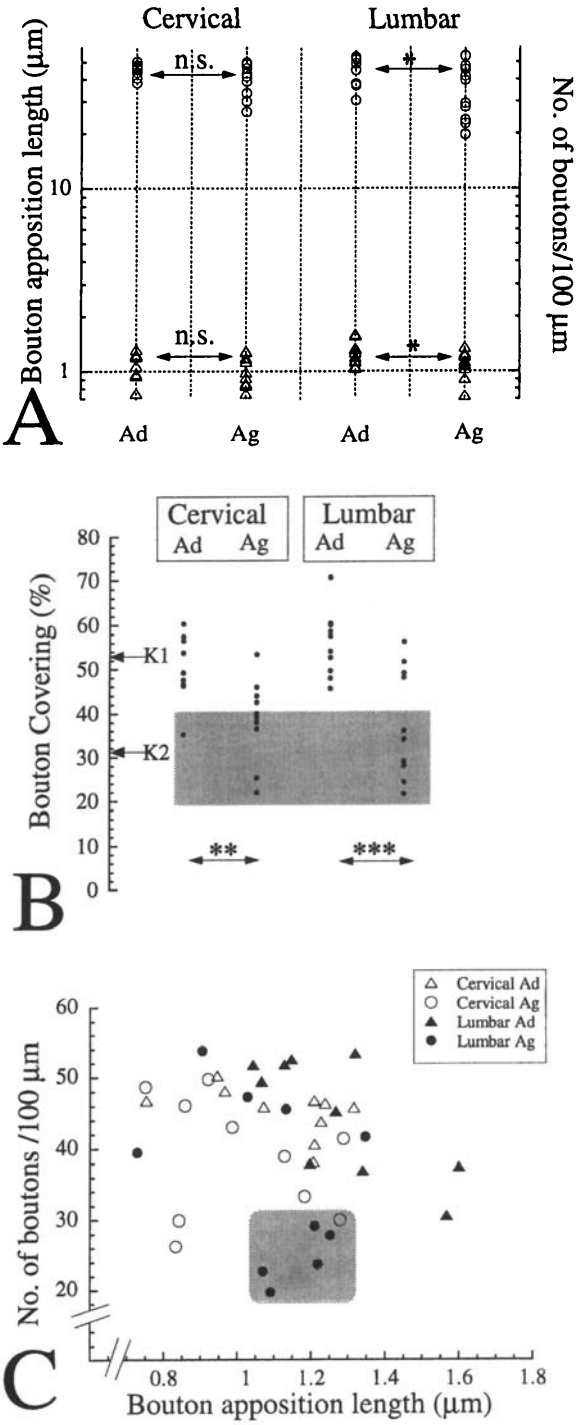

Figure 2. (**A**) Diagram showing the distribution of bouton apposition length (open triangles) and number of boutons/100 μm plasma membrane (open circles) for cervical and lumbar motoneurons of aged (Ag) and young adult (Ad) rats, respectively. Note logarithmic ordinate. Asterisks indicate level of significance (see *Materials and Methods*). (**B**) Distribution of bouton covering percentage in cervical and lumbar motoneurons of aged and young adult rats. K1 and K2 indicate cluster center, shaded area indicates region for observations with low covering values. Asterisks indicate level of significance (see *Material and Methods*). (**C**) Scattergrams showing the relation between mean apposition length (abscissa), on one hand, and number of bouton/100 μm plasma membrane (ordinate) on the other. The shaded area encloses observations from aged rats with low values for profile density and normal values for apposition length (for further details, see text). The frame contains the key to the symbols.

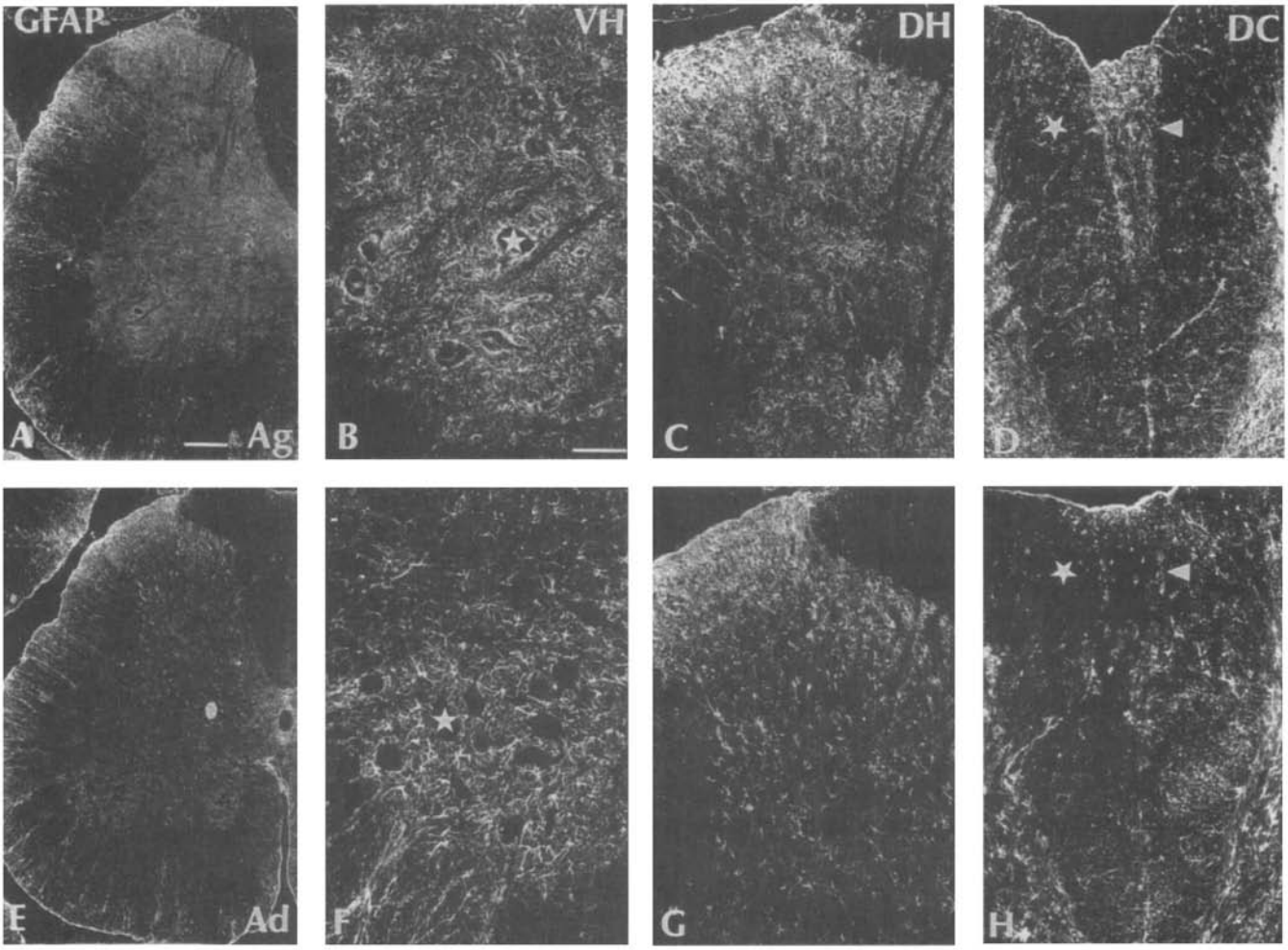

Figure 3. Micrographs showing the labeling pattern for GFAP-like IR in aged (Ag) (**A–D**) and young adult (Ad) (**E–H**) rats in the lumbar spinal cord. (**A** and **E**) An overview; note the increase in GFAP-like IR staining in **A** compared to **E**. (**B** and **F**) Higher power view of the ventral horn motor nucleus (asterisks indicate large neurons, presumably motoneurons). The density of GFAP-like IR processes is much higher in the aged rat and there is an accumulation of GFAP-like IR profiles around large neurons. (**C** and **G**) High power view of the dorsal horn. (**D** and **H**) High power view of the dorsal column. Note the increase in GFAP-like IR profiles in the medial part of the dorsal column (arrowheads) in **D** compared to **H**. Asterisks indicate the lateral portions of the dorsal columns. [Bars = 100 μm (**A** and **E**) and 50 μm (**B–D**, **F–H**).]

Loss of Axosomatic Input to Aged Motoneurons

We have used the method described by Conradi and Ronnevi [ref. 61; see also Conradi (51)] to examine changes in bouton covering of motoneurons. Bouton covering is a combined measurement of number of apposing boutons and the apposition length of the individual boutons. Based on the statistical analysis, it seems that the reduced values for synaptic covering in aged motoneurons were due mainly to a smaller number of bouton profiles. Because the size of the postsynaptic motoneurons did not vary systematically between aged and young adult rats, we deduced that, with all probability, many aged motoneurons have a smaller number of axosomatic boutons. This result is in agreement with data presented by Geinisman (25) from the dentate gyrus of aged rats. The loss of axosomatic boutons, however, is not general among motoneurons. It affects about 50% of the motoneurons in the present material (62). The affected neurons disclosed a decrease in bouton covering in the range of 25–60%. Furthermore, there seems to be a difference between spinal cord levels, with lumbar motoneurons being more severely affected. The differences in values recorded between the two aged rats were not statistically significant but may indicate a variability among members of the same age cohort. This is in line with observations in the basal forebrain of aged rats (62,63).

Although the mechanism(s) by which motoneurons become partially deprived of their axosomatic input cannot be answered here, it seems conceivable that the loss may be caused by aging-related lesions of afferent axons to the motoneurons and/or as a reaction to motor axon lesions. There is evidence in favor of both explanations. For example the extensive bulbospinal serotoninergic projection to spinal motoneurons (64,65) shows signs of fiber degeneration/dystrophy in aged rats (39,41). However, there is also strong evidence for motor axon degeneration/demyelination as well as axon losses (34–37,48,66–70). On the other

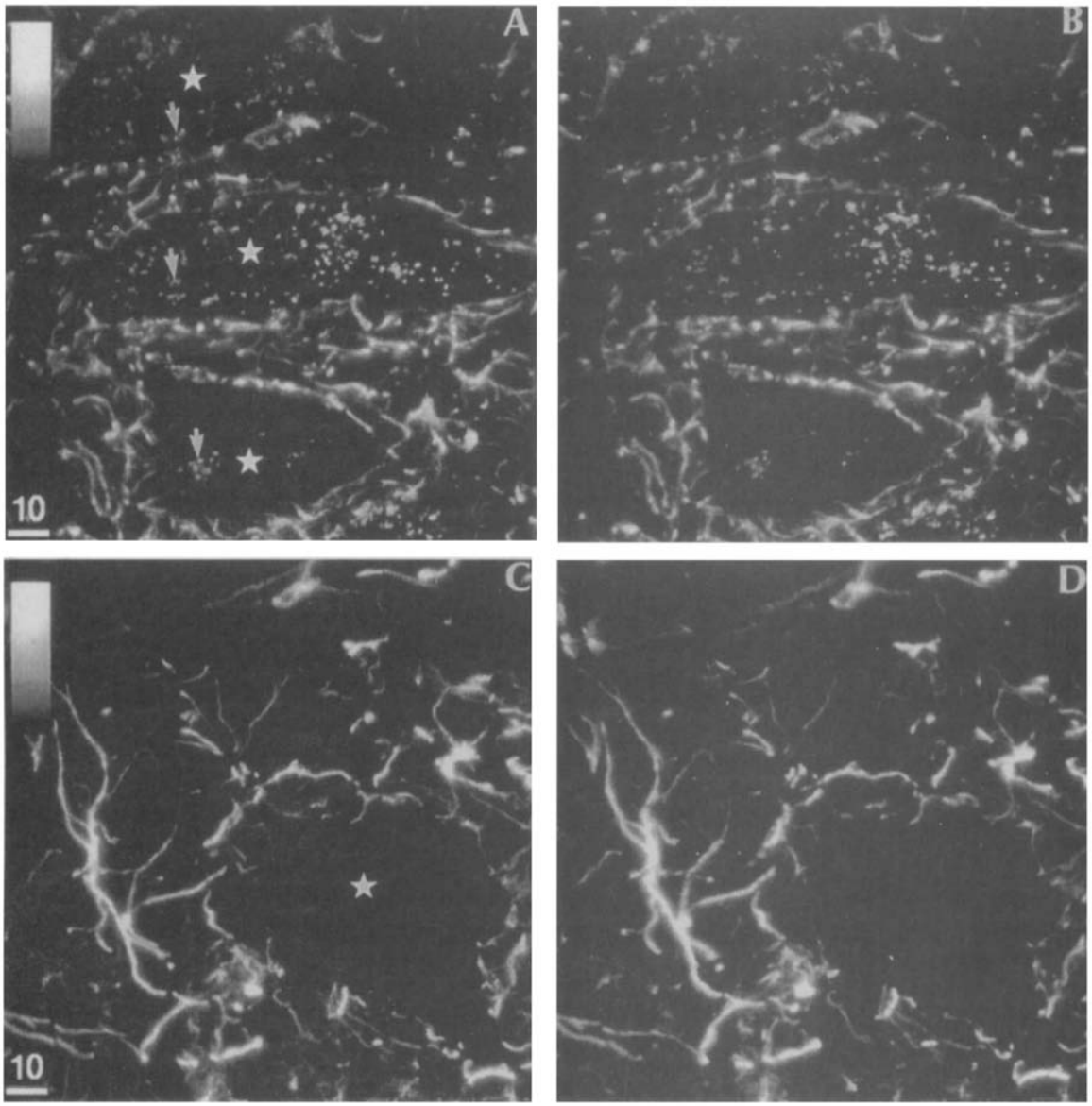

Figure 4. Stereo pairs (**A** and **B** and **C** and **D**) (8° between images) of confocal images. The image stacks comprise a volume of 80 × 80 × 8 μm each. (**A** and **B**) Three large neurons (asterisks) in the lateral lumbar motor nucleus from an aged rat, surrounded by dense accumulation of GFAP-IR processes. Numerous fluorescent lipofuscin-like pigments can be seen in the aged neurons (arrows). (**C** and **D**) A corresponding image from a young adult rat with one large neuron (asterisk). Note the classical radial distribution of the GFAP-IR profiles. Scale for gray-level intensities can be seen to the left in images **A** and **C**, respectively. (Scale = 10 μm.)

hand, counts of number of motoneurons in the spinal cord in aged individuals have only revealed small losses (10–20%) of motoneurons [refs. 38, 71, and 72; see, however, Hashizume et al. (69)]. Thus, it seems that spinal motoneurons suffer axonal insult during normal aging and therefore may react as young adult motoneurons subjected to axon severance (38).

Loss of synaptic boutons is a major event in the "axon reaction" following axonal severance [for a review, see Lieberman (73)]. In the axon reaction, the motoneuron is deprived of a large portion of its synaptic input [refs. 74 and 75; for a review, see Lieberman (73)]. This process starts at the cell body and involves glial cells, resulting in a decrease in both the number of boutons per unit membrane and bouton apposition length. After several weeks, the cell bodies are to a large extent covered by astrocytic processes (75,76,77) and at this time point regenerative forces start to restore the synaptic connectivity, which reaches about normal values after several months (H. Lindå, personal communication). Interestingly, during this cycle, the cell body plasma membrane shows complex changes, including sprout-/growth-like extensions (75,78). These are conspicuously similar to those found in the present material among aged motoneurons. In lumbar motoneurons, such plasma membrane irregularities were frequently associated with boutons and, thus, were suggested to be part of a regenerative/sprouting process initiated by the axon injury (75). We therefore suggest that the plasma membrane extensions observed here on aged rat motoneurons may represent a regenerative/restorative effort (28,79), whereas the loss of

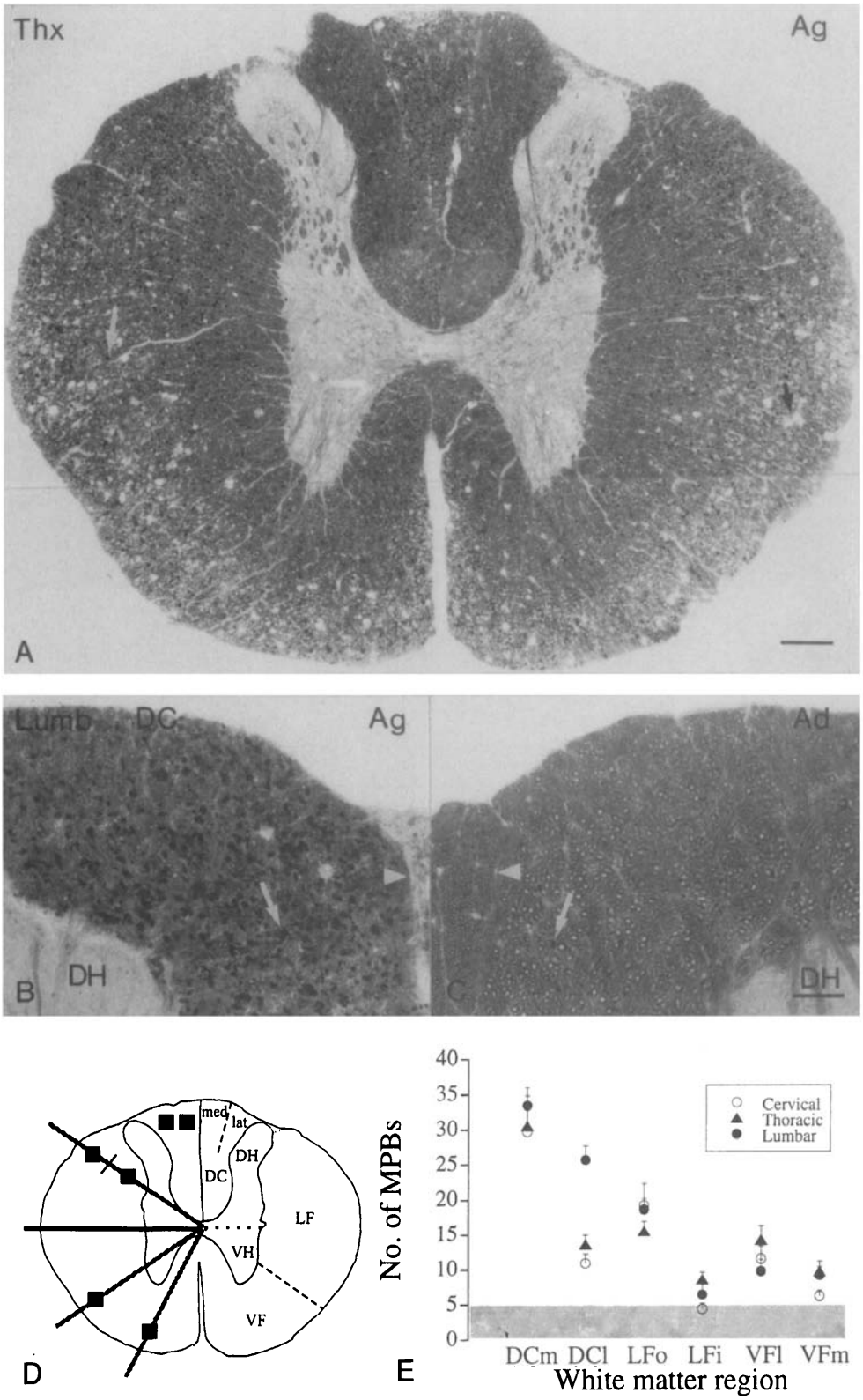

Figure 5. (**A**) Micrograph of a Marchi-stained section from a mid-thoracic segment in an aged rat. Note the numerous cystic enlargements (black arrow) and large numbers of MPBs (white arrow) in, especially, the peripheral parts of the VF and LF, and the medial part of the DC. (**B** and **C**) Dorsal columns of the lumbar spinal cord from an aged (**B**) and a young adult (**C**) rat. Note the large number of MPBs and the pale appearance, indicating a low myelin content, of the most medial part (arrowhead) of the dorsal column in the aged rat. [Bars = 220 μm (**A**) and 80 μm (**B** and **C**).] (**D**) Schematic drawing of the section in **A** showing the nomenclature used. Black squares indicate the regions within which the number of MPBs were counted (VF = ventral funiculus; LF = lateral funiculus; DC = dorsal column; med = medial portion of outer DC; lat = lateral portion of outer DC. (**E**) Diagram showing the mean (± *SEM*) number of MPBs in different regions of the white matter. Each symbol represents a spinal cord level. Shaded area indicates range of MPBs observed in young adult rats. DCm = dorsal column, medial portion; DCl = dorsal column, lateral portion; LFo = lateral funiculus, outer portion; LFi = lateral funiculus, inner portion; VFl = ventral funiculus, lateral portion; and VFm = ventral funiculus, medial portion.

input may have been triggered by aging-associated lesion of the motoneuron axon. This explanation to the observed changes could also fit with the fact that only a subpopulation of aged motoneurons was affected. It is more difficult to conceive that axon dystrophy/degeneration of afferent input, such as the bulbospinal serotoninergic pathway, would significantly influence only a subpopulation of the aged motoneurons.

Astrogliosis

The aged motoneurons that disclosed low values for bouton apposition showed a corresponding increase in apposing pale glial-like processes. GFAP immunohistochemistry revealed that, with all probability, the processes were astrocytic, and in some instances the aged motoneurons were "embedded" in GFAP immunopositive profiles. GFAP may therefore be a useful marker at the light microscopic level in studies of deafferentated motoneurons during aging. Astrogliosis is fairly widespread in the aging brain and spinal cord. It has been associated with loss of axon terminals as in this study, but also with synaptic remodeling (80). A number of studies have shown increased content of GFAP and GFAP mRNA in aged mouse, rat, and human brains (81–85). Our results in the aged rat spinal cord are in line with this. However, what triggers the astrogliosis and increased levels of GFAP around motoneurons during aging remains unresolved. One candidate signal molecule is calcitonin gene-related peptide (CGRP) (86), which is expressed in motoneurons and up-regulated in the cellular response to axon severance (86,87). In vitro experiments have shown that CGRP can activate astroglial cells (89). Moreover, CGRP binding sites are present on glial cells and CGRP can induce morphological changes in astrocytes (90). CGRP can also inhibit macrophage activation and thus possibly suppress inflammatory reactions triggered by degeneration/injury in the central nervous system. It is yet unresolved, however, if this signaling mechanism also operates in vivo. Furthermore, it is not known if microglial cells/macrophages are activated/involved in aging-related lesions (81). Nevertheless, a large number but not all spinal motoneurons in aged rats show a robust up-regulation of CGRP (38). Clearly, this issue deserves further attention.

In this study we also noted that some regions of the spinal cord white matter, in particular the dorsal columns, were sites of increased labeling for GFAP. Recently, examination of GFAP null mutant mice revealed derangement of white matter and abnormal myelination, indicating that GFAP (astrocytes) is important for oligodendrocyte function (91). The increased labeling for GFAP in the white matter of aged rats may be a response to oligodendroglial changes including myelin degeneration (92). In order to shed some light on this issue, we also examined Vibratome sections incubated with Marchi solution to reveal myelin and myelin breakdown components (MPBs) (50,93). White matter regions with large numbers of MPBs in aged rats appeared to coincide with regions disclosing intensive labeling for GFAP. The presence of large quantities of MPBs may indicate an increased breakdown of myelin, as during axon (Wallerian) degeneration. It cannot be excluded, however, that the increased occurrence of MPBs was due to changes in clearance-rate of myelin breakdown products (50,60). The weak Marchi staining and the absence of MPBs in the most medial part of the lumbar dorsal columns of aged rats may indicate that breakdown/elimination of myelin had caused depletion of myelin and myelin breakdown products.

Functional Consequences of a Reduced Axosomatic Input to Spinal Motoneurons

A decreased axosomatic input (19,40,41) may result in a decreased activation of the motoneurons and, as a consequence, inappropriate/decreased use of the muscle fibers. Furthermore, lumbar motoneurons should be more extensively affected than cervical motoneurons. In earlier studies (38,40) we found behavioral signs of motor dysfunction occurring in about 70–90% of the 30-month-old rats (34–37), which preferentially affects the hind limbs. A decrease in synaptic input to the parent motoneurons may have contributed to the observed incapacity.

ACKNOWLEDGMENTS

This study was supported by grants from the Swedish Medical Research Council (project 10820), L. and H. Ostermans fond för medicinsk forskning, Kapten A. Erikssons stiftelse, M. och A. Wallenbergs Minnesfond, and the Karolinska Institutet.

We thank Professor T. Hökfelt for advice and support and Professor Emeritus G. Grant for valuable comments on the manuscript.

Address correspondence to Dr. Susanna Kullberg, Department of Neuroscience, Karolinska Institutet, S-171 77 Stockholm, Sweden. E-mail: brun.ulfhake@neuro.ki.se

REFERENCES

1. Terry RD, DeTeresa R, Hansen LA. Neocortical cell counts in normal human adult aging. *Ann Neurol.* 1987;21:530–539.
2. Flood DG, Coleman PD. Neuron numbers and sizes in aging brain: comparison of human, monkey, and rodent data. *Neurobiol Aging.* 1988;9:453–463.
3. Peters A, Sethares C. Aging and the Meynert cells in the rhesus monkey primary visual cortex. *Anat Rec.* 1993;236:721–729.
4. Monji A, Morimoto N, Okuyama I, Umeno K, Nagatsu I, Ibata Y, Tashiro N. The number of noradrenergic and adrenergic neurons in the brain stem does not change with age in male Sprague-Dawley rats. *Brain Res.* 1994;641:171–175.
5. Peters A, Leahu D, Moss MB, McNally KJ. The effects of aging on area 46 of the frontal cortex of the rhesus monkey. *Cereb Cortex.* 1994;4:621–635.
6. Wickelgren I. For the cortex neuron loss may be less than thought. *Science.* 1996;273:48–50.
7. Bergman E, Ulfhake B. Loss of primary sensory neurons in the very old rat: neuron number estimates using the unbiased disector method and confocal optical sectioning. *J Comp Neurol.* 1998;in press.
8. Kim CB, Pier LP, Spear PD. Effects of aging on numbers and sizes of neurons in histochemically defined subregions of monkey striate cortex. *Anat Rec.* 1997;247:119–128.
9. Peinado MA, Quesada A, Pedrosa JA, Martinez M, Esteban FJ, Del Moral ML. Light microscopic quantification of morphological changes during aging in neurons and glia of the rat parietal cortex. *Anat Rec.* 1997;247:420–425.
10. Peters A, Nigro NJ, McNally KJ. A further evaluation of the effect of age on striate cortex of the rhesus monkey. *Neurobiol Aging.* 1997;18:29–36.
11. Vincent SL, Peters A, Tigges J. Effects of aging on the neurons within area 17 of rhesus monkey cerebral cortex. *Anat Rec.* 1989;223:329–341.
12. Palmer AM, DeKosky ST. Monoamine neurons in aging and Alzheimer's disease. *J Neural Transm.* 1993;91:135–159.

13. West MJ. Regionally specific loss of neurons in the aging human hippocampus. *Neurobiol Aging.* 1993;14:287–293.
14. Giannakopoulos P, Bouras C, Kovari E, Shioi S, Tezapsidis N, Hof PR, Robakis NK. Presenilin-1-immunopositive neurons are preserved in late-onset Alzheimer's disease. *Am J Pathol.* 1997;150:429–436.
15. Simic G, Kostovic I, Winblad B, Bogdanovic N. Volume and number of neurons of the human hippocampal formation in normal aging and Alzheimer's disease. *J Comp Neurol.* 1997;379:482–494.
16. Seitelberger F. Eine unbekannte form von infantiler Lipoid-Speicher-Krankheit des Gehirns. In: *Proceedings of the First International Congress of Neuropathology, Rome*, Vol. 3. Torino, Italy: Rosenberg & Sellier; 1952:323–333.
17. Fujisawa K, Shiraki H. Study of axonal dystrophy. I. Pathology of the neuropil of the gracile and the cuneate nuclei in aging and old rats: a stereological study. *Neuropathol Appl Neurobiol.* 1978;4:1–20.
18. Johnson JE, Mehler WR, Miquel J. A fine structural study of degenerative changes in the dorsal column nuclei of aging mice: lack of protection by vitamin E. *J Gerontol.* 1975;30:395–411.
19. Fujisawa K. Study of axonal dystrophy. III. Posterior funiculus and posterior column of aging and old rats. *Acta Neuropathol.* 1988;76: 115–127.
20. van Luijtelaar MGPA, Steinbusch HWM, Tonnaer JADM. Aberrant morphology of serotonergic fibers in the forebrain of the aged rat. *Neurosci Lett.* 1988;95:93–96.
21. Schmidt REL, Beaudet SB, Plurad WD, Snider Ruit KG. Pathologic alterations in pre- and postsynaptic elements in aged mouse sympathetic ganglia. *J Neurocytol.* 1995;24:189–206.
22. Jellinger K. Neuroaxonal dystrophy: its natural history and related disorders. In: Zimmerman HM, ed. *Progress in Neuropathology,* Vol. II. New York: Grune & Stratton; 1973:129–180.
23. Cotman CW, Holets VR. Structural changes at synapses with age: plasticity and regeneration. In: Schneider EL, Finch CE, eds. *Handbook of the Biology of Aging,* 2nd ed. New York: Van Nostrand Reinhold; 1985:617–644.
24. Bondareff W. Synaptic atrophy in the senescent hippocampus. *Mech Ageing Dev.* 1979;9:163–171.
25. Geinisman Y. Loss of axosomatic input in the dentate gyrus of aged rats. *Brain Res.* 1979;168:485–492.
26. Glick R, Bondareff W. Loss of synapses in the cerebellar cortex of the senescent rat. *J Gerontol.* 1979;34;818–822.
27. Uemura E. Age-related changes in prefrontal cortex of Macaca mulatta: synaptic density. *Exp Neurol.* 1980;69:164–172.
28. McWilliams JR, Lynch G. Synaptic density and axonal sprouting in rat hippocampus: stability in adulthood and decline in late adulthood. *Brain Res.* 1984;294:152–156.
29. Masliah E, Miller A, Terry RD. The synaptic organization of the neocortex in Alzheimer's disease. *Med Hypoth.* 1993;41:334–340.
30. Saito S, Kobayashi S, Ohashi Y, Igarashi M, Komiya Y, Ando S. Decreased synaptic density in aged brains and its prevention by rearing under enriched environment as revealed by synaptophysin contents. *J Neurosci Res.* 1994;39:57–62.
31. Martin LJ, Pardo CA, Cork LC, Price DL. Synaptic pathology and glial responses to neuronal injury precede the formation of senile plaques and amyloid deposits in the aging cerebral cortex. *Am J Pathol.* 1994;145:1358–1381.
32. Bertoni-Freddari C, Fattoretti P, Paoloni R, Caselli U, Galeazzi L, Meier-Ruge W. Synaptic structural dynamics and aging. *Gerontology.* 1996;42:170–180.
33. Kennel PF, Finiels F, Revah F, Mallet J. Neuromuscular function impairment is not caused by motor neurone loss in FALS mice: an electromyographic study. *NeuroReport.* 1996;7:1427–1431.
34. Berg BN, Wolf A, Simms HS. Degenerative lesions of spinal roots and peripheral nerves in ageing rats. *Gerontologia.* 1962;6:72–80.
35. van Steenis G, Kroes R. Changes in the nervous system and musculature of old rats. *Vet Pathol.* 1971;8:320–332.
36. Burek JD, van der Kogel AJ, Hollander CF. Degenerative myelopathy in three strains of aging rats. *Vet Pathol.* 1976;13:321–331.
37. Mitsumori K, Maita K, Shirasu Y. An ultrastructural study on spinal nerve roots and dorsal root ganglia in aging rats with spontaneous radiculoneuropathy. *Vet Pathol.* 1981;18:714–726.
38. Johnson H, Mossberg K, Arvidsson U, Piehl F, Hökfelt T, Ulfhake B. Increase in alpha-CGRP and GAP-43 in aged motoneurons: a study of peptides, growth factors and Chat mRNA in the lumbar spinal cord of senescent rats with symptoms of hind limb incapacities. *J Comp Neurol.* 1995;359:69–89.
39. Johnson H, Ulfhake B, Dagerlind Å, Bennett GW, Fone KC, Hökfelt T. The serotoninergic bulbospinal system and brainstem-spinal cord content of serotonin-, TRH-, and substance P-like immunoreactivity in the aged rat with special reference to the spinal cord motor nucleus. *Synapse.* 1993;15:63–89.
40. Johnson H, Mossberg K, Ulfhake B. The size number and fluorescence intensity of 5HT-immunoreactive axoh terminals in the aged rat lumbar spinal cord motor nucleus as revealed by confocal fluorescence microscopy and computerized 3D image analysis. In: Ulfhake B, Mossberg K, Carlsson K, eds. *A Companion to Methods in Neurosciences.* 1993:101–112.
41. Ramírez-León V, Kullberg S, Ottersen OP, Storm Mathisen J, Ulfhake B. Distribution of glutathione-, glutamate, GABA- and glycine-immunoreactivities in the aged rat spinal cord motor nucleus. 1998; in preparation.
42. Bergman E, Johnson H, Zhang X, Hökfelt T, Ulfhake B. Neuropeptides and neurotrophin receptor mRNAs in primary sensory neurons of aged rats. *J Comp Neurol.* 1996;375:303–319.
43. Uyeda CT, Eng LF, Bignami A. Immunological study of the glial fibrillary acidic protein. *Brain Res.* 1972;37:81–89.
44. Gutman B, Hanzlíková V. *Age Changes in the Neuromuscular System.* Bristol: Scientechnica; 1972.
45. Masoro EJ. Mortality and growth characteristics of rat strains commonly used in aging research. *Exp Aging Res.* 1980;6:219–233.
46. Burek JD, Hollander CF. Experimental gerontology. In: Baker HJ, Lindsey JR, Weisbroth SH, eds. *The Laboratory Rat,* Vol II. New York: Academic Press; 1980:149–159.
47. Algeri S, Calderini G, Toffano G, Ponzio F. Neurotransmitter alterations in aging rats. In: Samuel DEA, ed. *Aging of the Brain.* New York: Raven Press; 1983:227–243.
48. Krinke G. Spinal radiculoneuropathy in aging rats: demyelination secondary to neuronal dwindling? *Acta Neuropathol.* 1983;59:53–69.
49. Adams CWM. *Neurochemistry.* New York: Elsevier; 1965.
50. Franson P, Ronnevi L-O. Myelin breakdown and elimination in the posterior funiculus of the adult cat after dorsal rhizotomy: a light and electron microscopic qualitative and quantitative study. *J Comp Neurol.* 1984;223:138–151.
51. Conradi S. Ultrastructure and distribution of neuronal and glial elements on the motoneuron surface in the lumbosacral spinal cord of the adult cat. *Acta Physiol Scand Suppl.* 1969;332:5–48.
52. Pease PC. Buffered formaldehyde as a killing agent and primary fixative for electron microscopy. *Anat Rec.* 1962;142:342.
53. Zamboni I, De Martino C. Buffered picric acid-formaldehyde: a new, rapid fixative for electron microscopy. *J Cell Biol.* 1967;35:148A.
54. Coons AH. Fluorescent antibody methods. In: Danielli JF, ed. *General Cytochemical Methods.* New York: Academic Press; 1958: 399–422.
55. Hartman B, Zide D, Udenfriend S. The use of dopamine *b*-hydroxylase as a marker for the central noradrenergic nervous system in rat brain. *Proc Natl Acad Sci USA.* 1972;69:2722–2726.
56. Johnson GD, de C Nogueira Araujo GM. A simple method of reducing the fading of immunofluorescence during microscopy. *J Immunol Methods.* 1981;43:349–350.
57. Platt JL, Michael AF. Retardation of fading and enhancement of intensity of immunofluorescence by *p*-phenylenediamine. *J Histochem Cytochem.* 1983;31:840–842.
58. Debus E, Weber K, Osborn M. Monoclonal antibodies specific for glial fibrillary acidic (GFA) protein and for each of the neurofilament triplet polypeptides. *Differentiation.* 1983;25:193–203.
59. Ulfhake B, Carlsson K, Mossberg K, Wallén P. Preparation, staining and examination of nervous tissue in the confocal microscope. In: *Neuroscience Protocols,* Module 3, Amsterdam: Elsevier; 1994:65–92.
60. Franson P, Ronnevi L-O. Myelin breakdown in the posterior funiculus of the kitten after dorsal rhizotomy. A qualitative and quantitative light and electron microscopic study. *Anat Embryol.* 1989;180:273–280.
61. Conradi S, Ronnevi L-O. Spontaneous elimination of synapses on cat spinal motoneurons after birth: do half of the synapses on the cellbodies disappear? *Brain Res.* 1975;92:505–510.
62. Scheff SW, Scott SA, DeKosky ST. Quantitation of synaptic density in the septal nuclei of young and aged Fisher 344 rats. *Neurobiol Aging.* 1991;12:3–12.

63. Armstrong DM, Sheffield R, Buzsaki G, Chen KS, Hersh LB, Nearing B, Gage FH. Morphologic alterations of choline acetyltransferase-positive neurons in the basal forebrain of aged behaviorally characterized Fisher 344 rats. *Neurobiol Aging.* 1993;14:457–470.
64. Dahlström A, Fuxe K. Evidence for the existence of monoamine neurons in the central nervous systems. II. Experimentally induced changes in the intraneuronal amine levels of the bulbospinal neuron system. *Acta Physiol Scand.* 1965;62:5–36.
65. Arvidsson U, Ulfhake B, Cullheim S, Bergstrand A, Theodorson E, Hökfelt T. Distribution of ^{125}I-galanin binding sites, immunoreactive galanin, and its coexistence with 5-hydroxytryptamine in the cat spinal cord: biochemical, histochemical, and experimental studies at the light and electron microscopic level. *J Comp Neurol.* 1991;308: 115–138.
66. Gilmore SA. Spinal nerve root degeneration in aging laboratory rats: a light microscopic study. *Anat Rec.* 1972;174:251–257.
67. Mufson EJ, Stein DG. Degeneration in the spinal cord of old rats. *Exp Neurol.* 1980;70:179–186.
68. Sharma AK, Bajada S, Thomas PK. Age changes in the tibial and plantar nerves of the rat. *J Anat.* 1980;130:417–428.
69. Hashizume K, Kanda K, Burke RE. Medial gastrocnemius motor nucleus in the rat: age-related changes in the number and size of motoneurons. *J Comp Neurol.* 1988;269:425–430.
70. Knox CA, Kokmen E, Dyck PJ. Morphometric alteration of rat myelinated fibers with aging. *J Neuropathol Exp Neurol.* 1989;48:119–139.
71. Kawamura Y, O'Brien P, Okazaki H, Dyck PJ. Lumbar motoneurons of man. II. The number and diameter distribution of large- and intermediate-diameter cytons in "motoneuron columns" of spinal cord of man. *J Neuropathol Exp Neurol.* 1977;36:861–870.
72. Tomlinson BE, Irving D. The numbers of limb motoneurons in the human lumbosacral cord throughout life. *J Neurol Sci.* 1977;34: 213–219.
73. Lieberman AR. The axon reaction: a review of the principal features of perikaryal responses to axon injury. *Int Rev Neurobiol.* 1971;14: 49–124.
74. Blinzinger K, Kreuzberg GW. Displacement of synaptic terminals from regenerating motoneurons by microglial cells. *Z Zellforsch Mikroskop Anat.* 1968;85:145–157.
75. Lindå H, Cullheim S, Risling M. A light and electron microscopic study of intracellularly HRP-labeled lumbar motoneurons after intramedullary axotomy in the adult cat. *J Comp Neurol.* 1992; 318:188–208.
76. Graeber MB, Kreutzberg GW. Astrocytes increase in glial fibrillary acidic protein during retrograde changes of facial motor neurons. *J Neurocytol.* 1986;15:363–373.
77. Graeber MB, Kreutzberg GW. Delayed astrocyte reaction following facial nerve axotomy. *J Neurocytol.* 1988;17:209–220.
78. Engel AK, Kreuzberg GW. Neuronal surface changes in the dorsal vagal motor nucleus of the guinea pig in response to axotomy. *J Comp Neurol.* 1988;275:181–200.
79. Cotman CW, Scheff SW. Compensatory synapse growth in aged animals after neuronal death. *Mech Ageing Dev.* 1979;9:103–117.
80. Adams I, Jones DG. Synaptic remodeling and astrocytic hypertrophy in rat cerebral cortex from early to late adulthood. *Neurobiol Aging.* 1982;3:179–186.
81. Berciano MT, Andres MA, Calle E, Lafarga M. Age-induced hypertrophy of astrocytes in rat supraoptic nucleus: a cytological, morphometric, and immunocytochemical study. *Anat Rec.* 1995;243: 129–144.
82. Goss JR, Finch CE, Morgan DG. Age-related changes in glial fibrillary acidic protein mRNA in the mouse brain. *Neurobiol Aging.* 1991;12:165–170.
83. O'Callaghan JP, Miller DB. The concentration of glial fibrillary acidic protein increases with age in the mouse and rat brain. *Neurobiol Aging.* 1991;12:171–174.
84. Nichols NR, Day JR, Laping NJ, Johnson SA, Finch CE. GFAP mRNA increases with age in rat and human brain. *Neurobiol Aging.* 1993;14:421–429.
85. Wagner AP, Reck G, Platt D. Evidence that V+ fibronectin, GFAP and S100 β mRNAs are increased in the hippocampus of aged rats. *Exp Gerontol.* 1993;28:135–143.
86. Raivich G, Reddington M, Haas CA, Kreuzberg GW. Peptides in motoneurons. *Prog Brain Res.* 1995;104:3–20.
87. Arvidsson U, Cullheim S, Ulfhake B, Hökfelt T, Terenius L. Altered levels of calcitonin gene-related peptide (CGRP)-like immunoreactivity of cat lumbar motoneurons after chronic spinal cord transection. *Brain Res.* 1989;489:387–391.
88. Streit WJ, Dumoulin FL, Raivich G, Kreutzberg GW. Calcitonin gene-related peptide increases in rat facial motoneurons after peripheral nerve transection. *Neurosci Lett.* 1989;101:143–148.
89. Haas CA, Reddington M, Kreutzberg GW. Calcitonin gene-related peptide stimulates the induction of c-*fos* gene expression in rat astrocyte cultures. *Eur J Neurosci.* 1991;3:708–712.
90. Lazar P, Reddington M, Streit W, Raivich G, Kreutzberg GW. The action of calcitonin gene-related peptide on astrocyte morphology and cyclic AMP accumulation in astrocyte cultures from neonatal rat brain. *Neurosci Lett.* 1991;130:99–102
91. Liedtke W, Edelmann W, Bieri PL, Chiu FC, Cowan NJ, Kucherlapati R, Raine CS. GFAP is necessary for the integrity of CNS white matter architecture and long-term maintenance of myelination. *Neuron.* 1996;17:607–615.
92. Peters A. Age-related changes in oligodendrocytes in monkey of cerebral cortex. *J Comp Neurol.* 1996;371:153–163.
93. Hildebrand C. Ultrastructural and light-microscopic studies of the developing feline spinal cord white matter. II. Cell death and myelin sheath disintegration in the early postnatal period. *Acta Physiol Scand Suppl.* 1971;364:109–144.

Received November 4, 1997
Accepted February 18, 1998